coatings

MDPI

Article

Short- and Long-Term Wettability Evolution and Corrosion Resistance of Uncoated and Polymer-Coated Laser-Textured Steel Surface

Marjetka Conradi [1,*], Tina Sever [1], Peter Gregorčič [2] and Aleksandra Kocijan [1]

[1] Institute of metals and technology, Lepi pot 11, 1000 Ljubljana, Slovenia; tina.sever@imt.si (T.S.); Aleksandra.kocijan@imt.si (A.K.)

[2] Faculty of Mechanical Engineering, University of Ljubljana, Aškerčeva 6, 1000 Ljubljana, Slovenia; Peter.Gregorcic@fs.uni-lj.si

* Correspondence: marjetka.conradi@imt.si; Tel.: +386-1-4701-955; Fax: +386-1-4701-927

Received: 28 August 2019; Accepted: 17 September 2019; Published: 19 September 2019

Abstract: We present the results of one year observation of wetting and corrosion properties of nanosecond fiber laser-textured stainless steel, uncoated and coated with epoxy or FAS (fluoroalkylsilane)-TiO_2/epoxy. A comparative study was performed on samples kept under ambient conditions and in reduced air pressure and humidity. The results show the ability to induce wettability conversion from initially superhydrophilic to final superhydrophobic state either indirectly by ageing the uncoated laser-textured surface or directly by application of FAS-TiO_2/epoxy coating. The storage conditions significantly influenced the wettability development of uncoated laser-textured steel, i.e., the process of ageing was slowed down in reduced air pressure and humidity. Detailed surface chemical analysis revealed that adsorption of the organic matters from the surrounding media influences the wettability conversion and ageing. However, the ageing of the coated surfaces was not affected by the storage conditions. Corrosion stability of uncoated laser-textured surfaces was enhanced over time due to the wettability transition, depending on their morphology. Coatings represent a superior barrier over the texture and wettability with the stable long-term surface protection against aggressive media.

Keywords: stainless steel; laser surface engineering; wettability conversion; surface chemistry; polymer coatings

1. Introduction

Austenitic stainless steel is known as one of the most important engineering materials due to its high corrosion resistance combined with favorable mechanical properties, such as high tensile strength [1,2]. It is widely used in several applications in medicine, the food industry, and environmental or construction engineering. However, for applications in aquatic media or in other aggressive environments, such as a chloride ion-rich environment, it is extremely important to adjust the wetting properties of the steel surface to ensure its optimal performance. This prolongs the lifetime of the material, prevents corrosion, and consequently reduces the additional costs if the material cannot fulfil the demands of the operating conditions. Manipulation of surface wettability of metallic surfaces, therefore, still represents a scientific challenge in view of optimization of surface properties for specific end uses within economically acceptable limitations.

Generally, metals are covered with an oxide layer that tends to be (super)hydrophilic due to high surface energy of metallic oxides [3]. Therefore, to turn a surface (super)hydrophobic, the surface energy of metallic oxide surface has to be lowered. In this respect, one of the most addressed procedures is surface chemical modification by surface coatings [4,5]. Research has been focused

mostly on synthesis of multifunctional superhydrophobic coatings for water-repellent and self-cleaning applications [6–8], where (super)hydrophobicity is regulated through multiscale roughness structures formed by various nanoparticles, i.e., silica, TiO_2, ZnO, etc. [9–11]. Polymer coatings, on the other hand, present an effective physical barrier between the metal and the environment containing aggressive species, and serve as a reservoir for corrosion inhibitors that help the steel surface to resist attacks from aggressive species [12].

Recently, laser texturing has been addressed as one of the most promising approaches, in view of its flexibility, accuracy, chemical-free production, lack of tool wear, and negligible effect on the properties of bulk material. Several studies report on micro-, nano- or picosecond laser-structured metallic surfaces which are initially (super)hydrophilic and turn (super)hydrophobic in ambient conditions with time due to the adsorption of organic matters from the surrounding atmosphere over time [3,5,13–19].

The wettability conversion is strongly correlated to enhancing corrosion protective performance of surfaces [20,21]. It has been shown that the most effective and durable protection against corrosion in aggressive media is provided by superhydrophobic surfaces/coatings in combination with pre-existing oxide layers typical for specific metallic substrates [20]. Although several studies have been devoted to the examination of how processing parameters influence metallic-surface wettability and corrosion behavior, most of them were performed only within a short-term (two month) period [17,18,21,22]. In our previous work [19], we have shown that solely the short-term evaluation of superhydrophilic-to-hydrophobic transition after the laser texturing of metallic surface may lead to wrong conclusions. However, there is still a lack of analysis about how the transition of wettability influences the electrochemical properties and corrosion stability of uncoated or coated laser textured surfaces within the long-term (one year) period.

In this paper, we studied short- and long-term wettability evolution and corrosion resistance of uncoated laser-textured surfaces and laser-textured surfaces coated with epoxy and FAS-TiO_2/epoxy composite coating. We compared the ageing of surface properties of samples stored in two atmospheres: in ambient conditions and in a chamber with reduced air pressure and humidity. By monitoring the static water contact angles and detailed surface chemical analysis we evaluated the time-dependence of the wettability transition from a superhydrophilic to superhydrophobic state of uncoated laser-textured surfaces, as well as hydrophobic to superhydrophobic transition of coated laser-textured surfaces. Short- and long-term protective performance of uncoated and coated surfaces in chloride ion-rich environments were analyzed with potentiodynamic measurements.

2. Materials and Methods

Materials—Austenitic stainless steel AISI 316L (17% Cr, 10% Ni, 2.1% Mo, 1.4% Mn, 0.38% Si, 0.041% P, 0.021% C, <0.005% S in mass fraction) was used as a substrate. The steel sheet with a thickness of 1.5 mm was cut into discs of 25 mm diameter, which were cleaned with ethanol in ultrasonic bath.

A two-component USP Class VI biocompatible epoxy EPO-TEK 302-3M (EPOXY TECHNOLOGY, Inc., Billerica, MA, USA) was mixed in the wt.% ratio 100:45 and used as a coating. TiO_2 nanoparticles with mean diameters of 30 nm were provided by Degussa, Wilmington USA. Prior to coating preparation, nanoparticles were functionalized in 1 vol % ethanolic fluoroalkylsilane (Sigma-Aldrich, Darmstadt, Germany) or FAS ($C_{16}H_{19}F_{17}O_3Si$) solution to induce hydrophobic effect.

Laser Texturing of the Surfaces—The surfaces were laser-textured by using a fiber laser (SPI Lasers, Ltd., G4, SP-020P-A-HS-S-A-Y, Southampton, UK) with a wavelength of 1060 nm, pulse duration of 28 ns, and pulse energy of 0.2 mJ. The laser beam was led through a scanning head (Raylase, SS-IIE-10, Wessling, Germany) and an F-theta lens by a focal distance of 163 mm. Since the beam expander to attain a beam diameter on the lens of 7.5 mm was used, the beam spot size on the sample, placed in a focal position, equals 38 m (considering the beam quality parameter M^2 = 1.3). The beam was led over the surface, first in y (90°) and then in x direction (0°), by scanning velocity of 270 mm/s. The pulse repetition rate equaled 90 kHz. Thus, the two consecutive pulses were separated by 3 m

(92% overlapping). The scanning line separations were equal for x and y direction. The following different scanning line separations were used: $x = y = 25$, 50, 100 m.

Coatings Preparation—Two types of coatings were spin-coated on laser-textured steel surfaces: epoxy coating (E) and FAS-TiO_2 nanoparticle epoxy coating (FAS-TiO_2/E). FAS-TiO_2/E coatings were prepared by first spin coating 2 wt % ethanolic solution of FAS-TiO_2 nanoparticles, which were covered with epoxy layer. All the coatings were cured in an oven for 3 h at 65 °C.

Surface Characterization—Scanning electron microscopy (SEM) analysis using field emission SEM JEOL JSM-6500F (JEOL, Tokyo, Japan) was employed to investigate the morphology of the laser-textured surfaces and the laser-textured surfaces coated with E and FAS-TiO_2/E coating.

The X-ray photoelectron spectroscopy (XPS) analyses were carried out on the PHI-TFA XPS spectrometer produced by Physical Electronics Inc (Chanhassen, MN, USA). The analyzed area was 0.4 mm in diameter and the analyzed depth was about 3–5 nm. Sample surfaces were excited by X-ray radiation from monochromatic Al source at photon energy of 1486.6 eV. The survey wide energy spectra were taken with pass energy of analyzer of 187 eV in order to identify and quantify present elements on the surface. The high-energy resolution spectra were acquired with energy analyzer operating at resolution of about 0.6 eV and pass energy of 29 eV. Casa XPS® software (version 2.3.15) [23] was used for the detailed data processing.

The surface wettability was evaluated with static water contact angles (θ) on laser-textured, epoxy-coated, and FAS-TiO_2/epoxy-coated laser-textured surfaces by using a surface energy evaluation system (Advex Instruments s.r.o., Brno, Czech Republic). Water drops of 5 μL were deposited on at least three different spots of the substrates to avoid the influence of roughness and gravity on the shape of the drop. The drop contour was analyzed from the image of the deposited liquid drop on the surface and the contact angle was determined by using Young–Laplace fitting. To minimize the errors due to roughness and heterogeneity, the average values of the contact angles of the drop were measured approximately 20 s after the deposition. All the contact angle measurements were carried out at 22 °C and ambient humidity.

Optical 3D metrology system, model Alicona Infinite Focus (Alicona Imaging GmbH, Graz, Austria), was used for the laser-textured surface topography analysis. The 3D surface roughness parameters, including the average height of the selected area, S_a, were evaluated and calculated from the Alicona Infinite Focus using IF-MeasureSuite Version 5.1. At least three measurements per sample were performed at magnification 200×, with a lateral resolution of 0.9 μm and a vertical resolution of 50 nm. The size of the analyzed area was 1335×997 μm^2.

Electrochemical Measurements—Electrochemical measurements were carried out in a simulated physiological Hank's solution, containing 8 g/L NaCl, 0.40 g/L KCl, 0.35 g/L $NaHCO_3$, 0.25 g/L $NaH_2PO_4 \times 2H_2O$, 0.06 g/L $Na_2HPO_4 \times 2H_2O$, 0.19 g/L $CaCl_2 \times 2H_2O$, 0.41 g/L $MgCl_2 \times 6H_2O$, 0.06 g/L $MgSO_4 \times 7H_2O$, and 1 g/L glucose, at pH = 7.8 and room temperature. The solution was chosen for possible biomedical applications. We used three-electrode flat corrosion cells. The investigated specimen was employed as working electrode (WE), a saturated calomel electrode (SCE, 0.242 V vs. SHE, standard hydrogen electrode) as reference electrode (RE), and a platinum net as counter electrode (CE). The measurements were performed by using BioLogic Modular Research Grade Potentiostat/Galvanostat/FRA Model SP-300 with an EC-Lab Software (version 11.27). The potentiodynamic curves were recorded after 1 h sample stabilization at the open-circuit potential (OCP), starting the measurement at 250 mV vs. SCE more negative than the OCP. The potential was then increased, using a scan rate of 1 mV s^{-1}. All the measurements were repeated three times.

3. Results and Discussion

3.1. Surface Morphology

The modification of as-received stainless steel surface morphology after laser-texturing with different scanning line separations Δx and Δy (0°/90°) is shown in Figure 1. The 0°/90° scanning

strategy was used to obtain the same morphology in x and y direction and to ensure that the results are comparable to our previous work [21]. It is clearly visible that for scanning line separation $\Delta x = \Delta y = 100$ µm well-defined µ-channels with approximate size of the directly laser ablated area of 40-µm width were formed (Figure 1 a,b). For $\Delta x = \Delta y = 50$ µm, the µ-channels start to overlap but we can still recognize the x-y µ-channel pattern (Figure 1c,d). As already shown [19], the samples with the smallest scanning line separation, $\Delta x = \Delta y = 25$ µm, result in a rough surface with no characteristic µ-channel pattern (Figure 1e,f). A similar effect was observed also in the case of 0° scanning strategy with small scanning line separations [24].

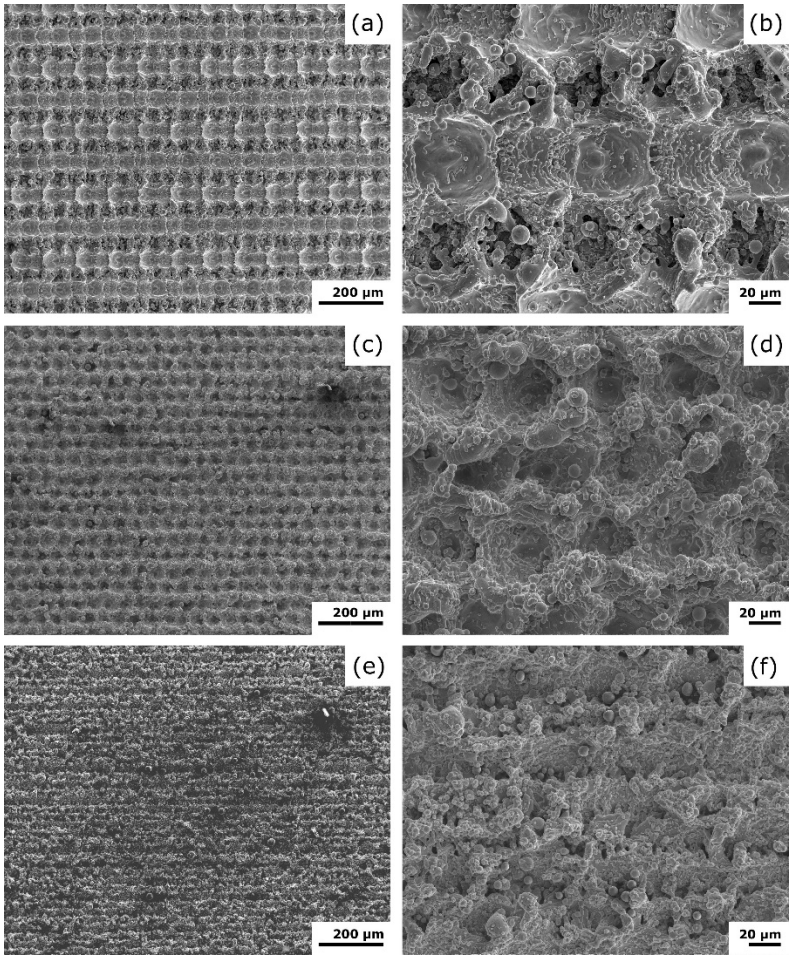

Figure 1. SEM micrographs of the laser-textured surfaces with different scanning line separations: (**a**,**b**) $\Delta x = \Delta y = 100$ µm, (**c**,**d**) $\Delta x = \Delta y = 50$ µm, (**e**,**f**) $\Delta x = \Delta y = 25$ µm.

After laser-texturing, some of the surfaces were additionally coated with pure epoxy coating (E) and some with epoxy coating enriched with FAS-functionalized 30 nm TiO_2 nanoparticles (FAS-TiO_2/E).

The average surface roughness parameter, S_a, and the rough surface areas were measured with Alicona Imaging System to evaluate the topographical differences between the laser-textured steel surfaces. As revealed in Table 1, the average surface roughness for the surfaces with $\Delta x = \Delta y = 100$ and 50 µm is of the same order of magnitude, $S_a = 10.8 \pm 0.1$ µm. S_a, however, drops for a factor of two for the surface with the smallest scanning line separation $\Delta x = \Delta y = 25$ µm. This indicates the increase of the laser-textured surface porosity, which is a consequence of the overlapped µ-channels [24]. The average surface roughness is, on the other hand, not affected by the application of epoxy and FAS-TiO_2/E coatings.

Table 1. Average surface roughness parameter S_a and the ratio between the rough and the smooth surface area, A_R/A_0 of uncoated and coated laser-textured surfaces.

Scan Line Separation $\Delta x = \Delta y$ [μm]	S_a [μm]	A_R/A_0
100 μm	10.8 ± 0.1	2.0 ± 0.3
100 μm, E	10.9 ± 0.1	1.7 ± 0.4
100 μm, FAS-TiO_2/E	11.2 ± 0.1	1.8 ± 0.2
50 μm	10.7 ± 0.1	4.3 ± 0.1
50 μm, E	10.4 ± 0.2	4.3 ± 0.2
50 μm, FAS-TiO_2/E	10.7 ± 0.2	4.1 ± 0.2
25 μm	5.2 ± 0.1	1.5 ± 0.1
25 μm, E	5.3 ± 0.2	1.4 ± 0.2
25 μm, FAS-TiO_2/E	5.6 ± 0.2	1.6 ± 0.2

The rough surface area was estimated through the ratio A_R/A_0 between the area of the rough, laser-textured surface, A_R and the smooth (unprocessed) surface, A_0. For the polished surface, the ratio $A_R/A_0 = 1$ and is increased due to laser ablation after laser texturing. This increase is important in characterization of the correlation between the developed rough surface and corrosion. The largest surface area results in a surface processed with $\Delta x = \Delta y = 50$ μm, while the surfaces processed with $\Delta x = \Delta y = 100$ and 25 μm have two to three times smaller surface, compared to $\Delta x = \Delta y = 50$ μm surface (Table 1).

3.2. Surface Wettability and Aging

We evaluated short-term (within three months) and long-term (after one year) development of the static water contact angles on uncoated, epoxy-coated and FAS-TiO_2/E-coated surfaces processed with scanning line separation $x = y = 100$, 50, and 25 m. The wettability evolution was compared for samples stored in two different media, in ambient conditions and in a chamber with reduced air pressure and humidity.

3.2.1. Uncoated Laser-Textured Surfaces

Similarly as in Ref. [15], the static water contact angle measurement immediately after the laser texturing showed that the surfaces were superhydrophilic in a saturated Wenzel regime ($\theta = 0°$) [18,25] for all scanning line separations. This means that the water droplets spilled into a thin film and completely wet the laser-textured surface. As shown in Figure 2, after initial superhydrophilicity, the surface wettability eventually starts to decrease, which is reflected in the increase of the contact angle. The surface first turns hydrophilic, then hydrophobic, until long-term stability of the superhydrophobicity is achieved for all scanning line separations in both storage media. This suggests a transition from Wenzel to Cassie–Baxter state due to the incomplete surface wetting after the static water contact angles saturate in a steady state [17]. Each measurement point in the graph represents the average of at least three individual measurements.

The contact angle evolution for all the samples can be well-fitted with exponential growth function, as shown in Figure 2, similar to Ref. [18]: $\frac{\theta}{\theta_0} = 1 - e^{-t/\tau}$. Here, θ_0 and τ are steady state contact angle and time constant, respectively, and are listed in Figure 2 and Table 2. The points were fitted from the day when the contact angle was above 0^o.

Even though we observed a similar trend in wettability development for all the surfaces, there was a clear difference in the progress of (super)hydrophobicity, depending upon scanning line separation as well as different storage media. The surface processed with $\Delta x = \Delta y = 100$ μm and stored in ambient conditions started to turn hydrophobic (measured non-zero contact angle) two days after laser texturing. Afterwards, we observed a characteristic 16-day transition period of hydrophobicity development with increasing contact angles of typically irregularly shaped droplets. An example of such irregularly shaped droplet development is shown in Figure 3; however it will be discussed in

detail in an independent study. Finally, the surface turned hydrophobic with observed spherically shaped droplets until reaching an equilibrium steady state superhydrophobicity.

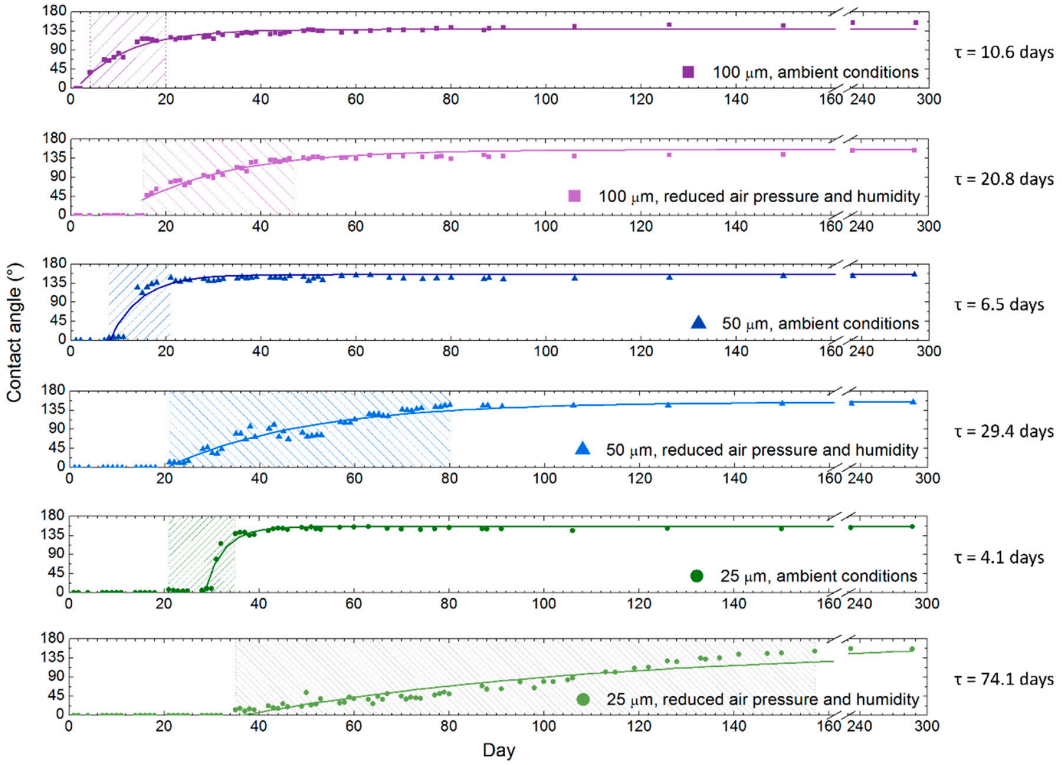

Figure 2. Short- and long-term development of static water contact angles with characteristic exponential growth fits and corresponding time constants of uncoated laser-textured steel surfaces with different scanning line separations ($\Delta x = \Delta y$ = 100, 50, 25 μm), stored in ambient conditions and in a chamber with reduced air pressure and humidity.

Table 2. Comparison of wettability development with corresponding time constants on samples stored in ambient conditions and in a chamber with reduced air pressure and humidity: time evaluation of complete wetting regime and transition period.

Scan Line Separations [μm]	Complete Wetting Regime	Transition Period	Time Constant, τ
100, ambient	4 days	16 days	10.6 days
100, chamber	15 days	31 days	20.8 days
50, ambient	8 days	13 days	6.5 days
50, chamber	21 days	59 days	29.4 days
25, ambient	21 days	14 days	4.1 days
25, chamber	35 days	122 days	74.1 days

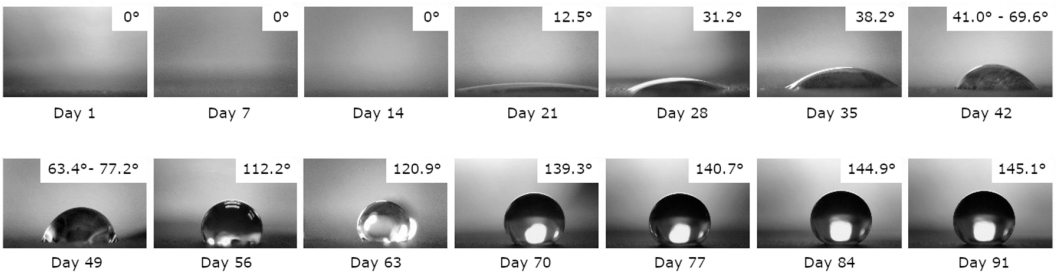

Figure 3. A typical example of droplet evolution from superhydrophilic to superhydrophobic state, through a phase with characteristic irregularly shaped droplets, on uncoated laser-textured surface with $\Delta x = \Delta y$ = 50 μm.

Surfaces stored in ambient conditions and processed with $\Delta x = \Delta y = 50$ and 25 μm started to turn hydrophobic after 8 and 21 days, respectively. On both samples, hydrophobicity was developing for approximately two weeks, similarly as described above, until the contact angle gradually reached a steady state contact angle of 146.3° ± 2.1° on a surface with $\Delta x = \Delta y = 50$ μm, whereas surface with $\Delta x = \Delta y = 25$ μm became superhydrophobic with a contact angle of 150.7° ± 2.3°. The two week transition period is also for surfaces with $\Delta x = \Delta y = 50$ and 25 μm, characterized with irregularly shaped droplets (Figure 3).

In a chamber with reduced air pressure and humidity, we observed that the process of hydrophobicity development of uncoated laser-textured surfaces for all scanning line separations was significantly slowed down, which is reflected also in larger time constants. As shown in Figure 2 and Table 2, hydrophobicity starts to develop with, approximately, a two week delay for all the samples stored in a chamber compared to the corresponding samples stored in ambient conditions. Afterwards, the hydrophobicity on samples stored in a chamber starts to increase, similarly as on samples stored in the ambient conditions. However, the time needed to achieve the saturated contact angle (the transition period) was prolonged (Table 2).

These results suggest that scanning line separation, together with the reduced air pressure and humidity, slow down surface ageing and the wettability conversion. In ambient conditions, the decrease of the scanning line separation postponed the start of the hydrophobicity development. However, the transition period before reaching saturation of the contact angle values was approximately the same for all the samples, i.e., 2 weeks (Table 2). Besides that, the smaller the scanning line separation, the steeper the increase of the contact angle to the steady state. In a chamber, the start of the hydrophobicity development is postponed with the decrease of the scanning line separation in the same manner as in ambient conditions.

To understand the mechanism of the ageing of uncoated laser-textured steel surfaces with time-dependent wettability conversion from superhydrophilic to superhydrophobic state, comparison of XPS surface chemical analysis of samples immediately after the preparation and after one year was evaluated. We performed deconvolution of C 1*s*, O 1*s*, Fe $2p_{3/2}$, Cr $2p_{3/2}$, Mo 3*d*, and Ni 2*p* peaks to analyze the surface state and the amount of carbon and other elements in the top layer. Deconvolution of all C peaks was performed by using fitting procedure after subtraction of a Shirley's background correction. The shape of all peaks was kept to be Gaussian/Lorentzian 60/30 ratio. C 1*s* peak was fitted with three species. The main peak around 284.7 eV was attributed to the hydrocarbon chains (C–C/C–H). The C–O represented the carbon bonded to one oxygen and C=O represented the double bond between carbon and oxygen, at 1.4–1.5 and 2.8–3.1 eV from the C–C/C–H components, respectively [26,27]. Figure 4 presents the examples of the deconvoluted XPS spectra of C 1*s*, O 1*s*, Fe $2p_{3/2}$, and Cr $2p_{3/2}$ laser-textured AISI 316L surface with $\Delta x = \Delta y = 50$ μm stored in ambient conditions immediately after preparation.

As shown in Figure 5, the composition of surface functional groups of laser-textured surfaces ($\Delta x = \Delta y = 25$, 50, and 100 μm) changed considerably on aged samples after one year, compared to samples immediately after preparation. To see these changes, the relative amounts of nonpolar C–C/C–H groups and metal oxides (M–O) were evaluated. The results show significantly higher amount of C–C/C–H groups on aged samples (Figure 5a). Due to their nonpolar nature, they serve as hydrophobic regions on the surface and therefore influence the wettability greatly. We should however stress that in spite of the presence of minor polar peak attributed to C–O and C=O groups on laser-textured surface immediately after the preparation, as well as after one year (Figure 5c), which serve as hydrophilic regions, wettability conversion from the initial superhydrophilicity to the final superhydrophobicity was observed on all uncoated laser-textured samples. Initial superhydrophilicity of laser-textured steel surfaces can be explained by a large number of polar sites originating from the presence of surface metal oxides, the amount of which decreases after one year (Figure 5b) [5,18]. The detected amount of nonpolar carbon immediately after the preparation is too small to shield the hydrophilicity of the surface oxides. Therefore, the intrinsic hydrophilicity of the polar metal oxides is

amplified by the laser-induced surface roughness according to Wenzel's theory. The conversion of surface wettability, on the other hand, is known to be caused by the adsorption of organic matters from the surrounding atmosphere over time [5,28]. This was confirmed by evaluating the atomic ratio between carbon and metal species (C/M), which is governed by the amount of adsorbed organic matters (Figure 5b). Finally, higher amount of C–C/C−H groups, lower amount of metal oxides, and higher C/M ratio on aged samples lead to more nonpolar (super)hydrophobic surface (Figure 5a,d).

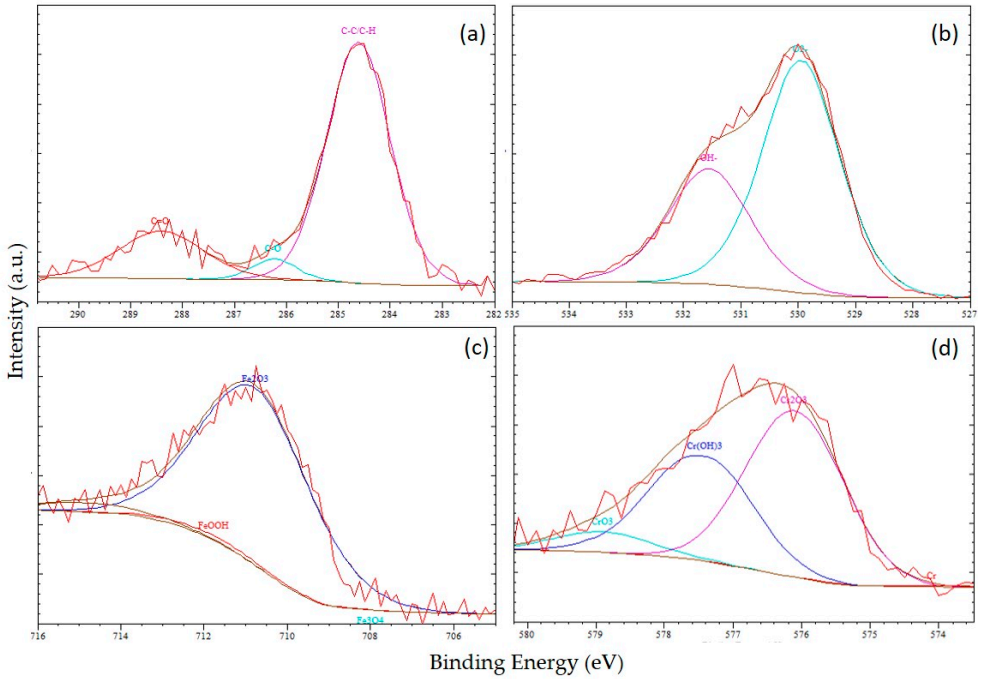

Figure 4. Deconvoluted XPS spectra of C 1*s* (**a**), O 1s (**b**), Fe $2p_{3/2}$ (**c**), Cr $2p_{3/2}$ (**d**) laser-textured AISI 316L surface $\Delta x = \Delta y = 50$ µm stored in ambient conditions immediately after preparation.

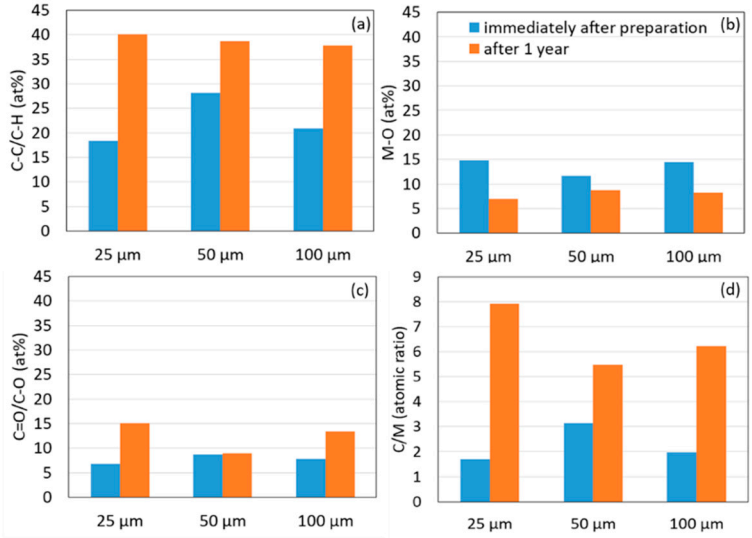

Figure 5. Relative amount of C–C/C–H functional groups (at.%) (**a**), relative amount of metal oxides M–O (**b**), relative amount of C=O/C–O (**c**), and the ratio of C/M obtained from the high-resolution XPS spectra (**d**) for laser-textured surfaces with $\Delta x = \Delta y = 25$, 50, and 100 µm.

3.2.2. Coated Laser Textured Surfaces

On coated laser-textured steel surfaces, no wettability conversion was observed. Depending on the scan line separation, the laser-textured surfaces coated with epoxy were immediately after preparation poorly (for $\Delta x = \Delta y = 100$ µm, 97.5° ± 1.4°) to moderately hydrophobic (for $\Delta x = \Delta y = 50$ and 25 µm; 112.1° ± 1.9° and 108.3° ± 2.3°, respectively). FAS-TiO_2/E-coated laser-textured surfaces were, however, strongly hydrophobic for $\Delta x = \Delta y = 100$ µm (143.4° ± 3.1°) and superhydrophobic for $\Delta x = \Delta y = 50$ and 25 µm (151.1° ± 2.1° and 151.9° ± 0.7°, respectively).

Short- and long-term contact angle development on epoxy-coated and FAS-TiO_2/E-coated laser-textured steel surfaces in ambient conditions and in a chamber with reduced air pressure and humidity is presented in Figure 6. Epoxy-coated samples stored in air and in a chamber remained poorly hydrophobic with a measured slight increase (few degrees, <10°) of contact angles on a short- and long-term basis for all scanning line separations (Table 3). FAS-TiO_2/E-coated surfaces in both media and for all scanning line separations turned or remained superhydrophobic on a short- and long-term basis again with a slight increase of contact angles (<5°) after a one year measurement period (Table 3). These results, therefore, indicate the long-term stability of coatings with stable and predictable wettability.

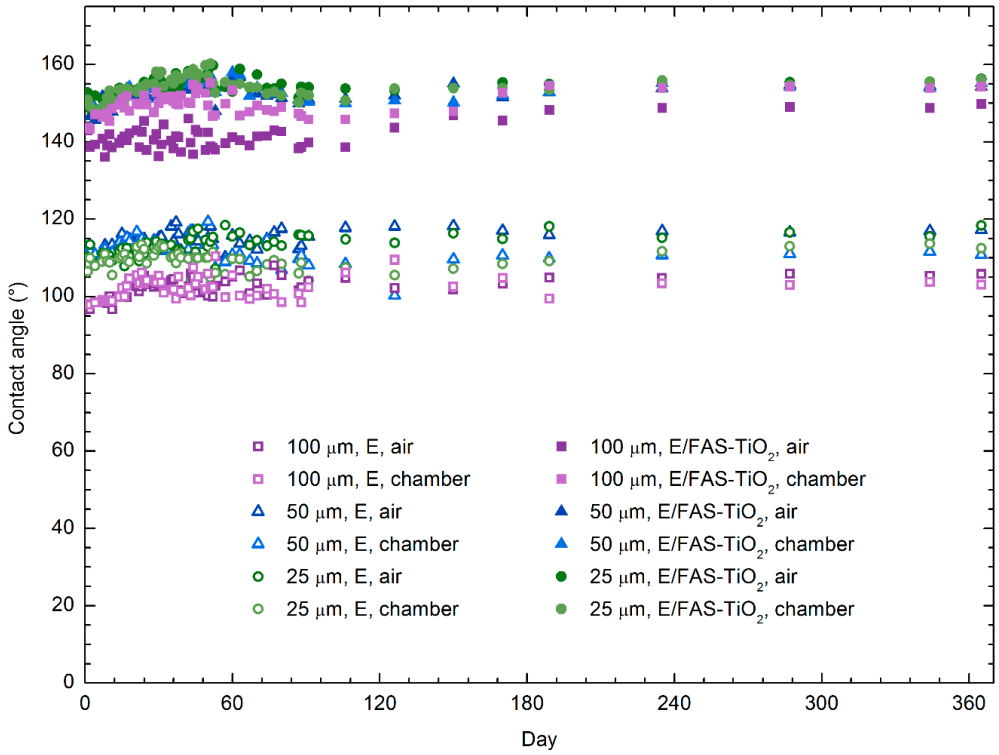

Figure 6. Time development of static water contact angles of epoxy-coated and FAS-TiO_2/E-coated laser-textured steel surfaces for different scan line separations ($\Delta x = \Delta y = 100$, 50, 25 µm) stored in ambient conditions and in a chamber with reduced air pressure and humidity.

Table 3. Comparison of static water contact angles of uncoated, epoxy-, and FAS-TiO_2/E-coated samples with different scan line separations ($\Delta x = \Delta y$ = 100, 50, 25 μm) measured immediately after preparation, after 3 months, and after 1 year, when stored in ambient conditions and in a chamber with reduced air pressure and humidity.

Scan Line Separation [μm]	Uncoated Contact angle [°]	E Contact Angle [°]	FAS-TiO_2/E Contact Angle [°]
Immediately after preparation			
100, ambient	0	97.5 ± 1.4	143.4 ± 3.1
50, ambient	0	112.1 ± 1.9	151.1 ± 2.1
25, ambient	0	108.3 ± 2.3	151.9 ± 0.7
3 months after preparation			
100, ambient	130.5 ± 0.6	104.3 ± 2.6	140.5 ± 2.2
100, chamber	138.6 ± 3.2	100.2 ± 1.7	147.3 ± 1.2
50, ambient	146.3 ± 1.6	115.0 ± 2.2	151.1 ± 0.9
50, chamber	145.1 ± 1.6	108.8 ± 1.5	151.5 ± 1.0
25, ambient	150.7 ± 1.1	115.0 ± 1.2	153.7 ± 1.3
25, chamber	56.5 ± 7.8	107.3 ± 2.2	152.0 ± 1.1
1 year after preparation			
100, ambient	154.5 ± 1.5	105.8 ± 2.2	149.8 ± 1.9
100, chamber	155.3 ± 1.8	103.0 ± 2.1	154.3 ± 0.9
50, ambient	155.1 ± 2.1	117.3 ± 1.6	154.2 ± 1.6
50, chamber	154.2 ± 2.1	110.8 ± 2.2	155.1 ± 1.2
25, ambient	155.8 ± 1.8	118.4 ± 1.9	156.3 ± 1.8
25, chamber	156.3 ± 1.6	112.5 ± 1.8	156.1 ± 1.5

3.3. Electrochemical Measurements

We evaluated potentiodynamic behavior of laser-textured uncoated, epoxy-, and FAS-TiO_2/epoxy-coated stainless steel processed with scan line separation $x = y$ = 100, 50, and 25 m in a simulated physiological Hank´s solution measured immediately after preparation, after three months, and one year when stored in ambient conditions (Figure 7). The polarization and the passivation behavior of the tested materials were significantly affected by the surface modification.

As shown in Figure 7a,d,g, immediately after preparation, the epoxy-, and FAS-TiO_2/epoxy-coated surfaces exhibited improved corrosion resistance with considerably broader range of passivation, which was also shifted to the lower corrosion–current densities, compared to uncoated surfaces. The observed shift was most pronounced for surfaces processed with $x = y$ = 25 m. The corrosion parameters calculated from the potentiodynamic measurements indicated that the corrosion stability of coated specimens significantly increased, including lower corrosion–current densities (i_{corr}), lower corrosion rates (v_{corr}), and higher polarization resistances (R_p), compared to uncoated specimens (Table 4). The ratio between the smooth and the rough surface area, $A_0/A_{R,}$ listed in Table 1 was implemented in calculation of i_{corr} and v_{corr}. The electrochemical evaluation of surfaces exposed to the ambient conditions showed the enhanced short- and long-term corrosion stability of uncoated and coated laser-textured surfaces prepared under the same experimental conditions (Figure 7b,c,e,f,h,i).

Uncoated laser-textured surfaces, immediately after the laser texturing, that exhibited superhydrophilic nature (Table 4) showed similar corrosion resistance for all scanning line separations ($x = y$ = 100, 50, and 25 m) (Table 4). This indicates that wetting properties dominate over the surface texture. After ageing, when the surfaces became (super)hydrophobic, we observed surface texture-dependent corrosion behavior. After three months, surfaces processed with scanning line

separation $x = y = 50$ m showed better corrosion resistance compared to $x = y = 100$ m and 25 m. As shown in Figure 1, surfaces processed with $x = y = 100$ m have a well-defined structure with a partly unprocessed steel surface, which is more susceptible to corrosion. On the other hand, the surfaces processed with $x = y = 25$ m were highly porous, which enabled the penetration of the aggressive ions, leading to the increased corrosion. This suggests that the surfaces processed with $x = y = 50$ m offer the best compromise between the laser texturing and, consequently, porosity. After one year, the corrosion resistance was further increased, since the increased long-term static contact angles reach superhydrophobic values on all the investigated uncoated laser-textured surfaces (Table 4). As the contact angles converge to similar values, we would expect similar corrosion resistance for all the aged uncoated laser-textured surfaces. However, corrosion resistance of $x = y = 25$ m surface remained lower due to high porosity, compared to well defined $x = y = 50$ and 100 m surfaces, which exhibited comparable corrosion stability. Observed long-term corrosion resistance of uncoated laser-textured surfaces is, therefore, effected not only by wetting properties of the surfaces but also by their morphology and imperfections, as reported by Boinovich et al. [20].

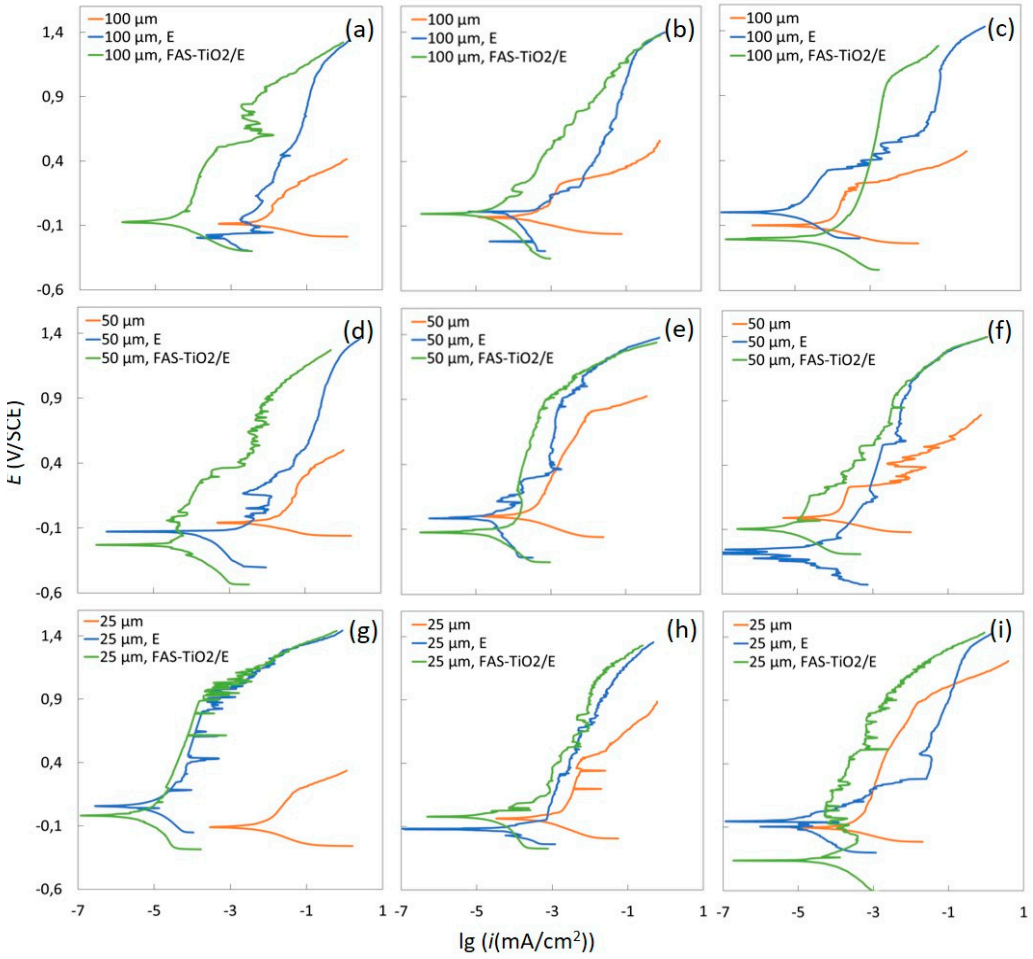

Figure 7. Potentiodynamic curves for uncoated, epoxy-coated, and FAS-TiO_2/epoxy-coated laser-textured stainless steel with different scan line separations ($\Delta x = \Delta y = 100, 50, 25$ µm) in a simulated physiological Hank´s solution measured (**a**,**d**,**g**) immediately after laser-texturing, (**b**,**e**,**h**) after 3 months, and (**c**,**f**,**i**) after 1 year storage in ambient conditions.

Table 4. Corrosion characteristics of uncoated, epoxy-coated and FAS-TiO_2/epoxy-coated laser-textured steel surfaces with different scan line separations ($\Delta x = \Delta y$ = 100, 50, 25 μm) calculated from the electrochemical measurements in a simulated physiological Hank´s solution and corresponding static water contact angles immediately after laser-texturing, after 3 months, and 1 year, when stored in ambient conditions.

Scan Line Separation [μm]	E_{corr} [mV]	i_{corr} [μA/cm^2]	v_{corr} [μm/year]	Contact Angle [º]
Immediately after preparation				
100 μm	−86.6 ± 0.5	4.345 ± 0.008	16.25 ± 0.07	0
100 μm, E	−172.9 ± 0.6	2.500 ± 0.006	3.45 ± 0.05	97.5 ± 1.4
100 μm, FAS-TiO_2/E	−70.7 ± 0.4	0.010 ± 0.001	0.25 ± 0.04	143.4 ± 3.1
50 μm	−59.7 ± 0.3	2.402 ± 0.005	20.51 ± 0.08	0
50 μm, E	−127.7 ± 0.5	0.209 ± 0.004	0.58 ± 0.03	112.1 ± 1.9
50 μm, FAS-TiO_2/E	−230.4 ± 0.9	0.007 ± 0.001	0.07 ± 0.01	151.1 ± 2.1
25 μm	−108.8 ± 0.5	5.540 ± 0.009	39.73 ± 0.07	0
25 μm, E	55.9 ± 0.2	0.013 ± 0.001	0.13 ± 0.01	108.3 ± 2.3
25 μm, FAS-TiO_2/E	−17.6 ± 0.1	0.002 ± 0.001	0.07 ± 0.01	151.9 ± 0.7
3 months after preparation				
100 μm	−30.6 ± 0.2	0.130 ± 0.007	0.70 ± 0.03	130.5 ± 0.6
100 μm, E	0.6 ± 0.1	0.155 ± 0.008	1.20 ± 0.04	104.3 ± 2.6
100 μm, FAS-TiO_2/E	−4.6 ± 0.1	0.005 ± 0.001	0.15 ± 0.01	140.5 ± 2.2
50 μm	1.6 ± 0.1	0.040 ± 0.004	0.42 ± 0.02	146.3 ± 1.6
50 μm, E	−11.1 ± 0.1	0.005 ± 0.001	0.12 ± 0.01	115.0 ± 2.2
50 μm, FAS-TiO_2/E	−121.4 ± 0.9	0.005 ± 0.001	0.05 ± 0.01	151.1 ± 0.9
25 μm	−35.7 ± 0.2	0.367 ± 0.006	2.60 ± 0.05	150.7 ± 1.1
25 μm, E	−120.3 ± 0.7	0.067 ± 0.003	0.40 ± 0.02	115.0 ± 1.2
25 μm, FAS-TiO_2/E	−20.4 ± 0.1	0.013 ± 0.002	0.27 ± 0.03	153.7 ± 1.3
1 year after preparation				
100 μm	−105.0 ± 0.9	0.015 ± 0.002	0.15 ± 0.01	155.3 ± 1.8
100 μm, E	−4.9 ± 0.8	0.005 ± 0.001	0.05 ± 0.01	103.0 ± 2.1
100 μm, FAS-TiO_2/E	−210.7 ± 0.9	0.035 ± 0.004	0.15 ± 0.01	154.3 ± 0.9
50 μm	−8.4 ± 0.1	0.009 ± 0.001	0.09 ± 0.01	154.2 ± 2.1
50 μm, E	−298.8 ± 0.3	0.009 ± 0.001	0.12 ± 0.01	110.8 ± 2.2
50 μm, FAS-TiO_2/E	−96.6 ± 0.5	0.002 ± 0.001	0.02 ± 0.01	155.1 ± 1.2
25 μm	−122.5 ± 0.6	0.127 ± 0.009	1.47 ± 0.02	156.3 ± 1.6
25 μm, E	−50.8 ± 0.9	0.007 ± 0.001	0.07 ± 0.01	112.5 ± 1.8
25 μm, FAS-TiO_2/E	−366.4 ± 0.3	0.060 ± 0.005	0.53 ± 0.05	156.1 ± 1.5

Corrosion resistance of coated surfaces immediately after preparation was, on the other hand, a combination of both wettability and surface morphology. We observed increased corrosion stability with decreased scanning line separation and the highest corrosion resistance was observed for FAS-TiO_2/epoxy-coated surface with $x = y$ = 25 and 50 m, which coincides with increased superhydrophobicity. After three months and one year, surfaces processed with $x = y$ = 100 m and 50 m and coated with E and FAS-TiO_2/E showed improved corrosion resistance compared to the samples

immediately after the preparation. This suggests the superior role of protective coatings over the laser texturing and wettability. The contact angles of E-coated surfaces were slightly increased with time and remained moderately hydrophobic, whereas the wettability of FAS-TiO_2/E remained practically unchanged, i.e., superhydrophobic. The corrosion resistance for coated $x = y = 25$ m surfaces was, however, mainly decreased. This indicates that its highly porous structure leads to possible penetration of chloride ions to the metal surface under the coating, which increases the corrosion. Due to very stable wettability on a short- and long-term basis (Table 4), stable, long-term corrosion resistance can be, in general, attributed to long-term durability of coatings, which maintain high barrier properties. However, in some cases discrepancies from this trend were observed due to the coatings' imperfections.

4. Conclusions

Nanosecond laser texturing of austenitic stainless steel surfaces followed by surface modification with organic coating was used to fabricate surfaces with different surface characteristics, morphology, and wettability. Surface morphology was regulated by variation of the scanning line separation, whereas short-term and long-term wettability and corrosion resistance was evaluated and compared for uncoated laser-textured steel surfaces, epoxy-coated, and FAS-TiO_2/epoxy-coated textured steel surfaces in two storage media, i.e., in ambient conditions and in a chamber with reduced air pressure and humidity. With wettability evolution, we have shown two successful ways of creating a superhydrophobic surface: (i) indirectly by controllable ageing of the uncoated laser-textured steel surfaces in two different atmospheres, ambient conditions, and in a chamber with reduced air pressure and humidity; and (ii) directly by application of epoxy/FAS-TiO_2 coatings on laser-textured steel surfaces in both storage media. Storage conditions, air vs. reduced air pressure, and humidity strongly influence the wetting characteristics and wettability development of uncoated laser-textured steel. Reduced air pressure and humidity slow down the ageing process and superhydrophilic to superhydrophobic wettability transition. XPS analysis revealed the nature of the wettability conversion of uncoated laser-textured steel by adsorption of organic matters from surrounding media. Coated laser-textured samples, on the other hand, retained wetting properties over time in both media, leading to long-term stability of coatings with predictable wettability. Corrosion stability of uncoated laser-textured surfaces became laser pattern-regulated after wettability conversion. In general, stability was enhanced over time due to surfaces' superhydrophobicity. However, it was regulated also by their morphology and imperfections. The results show that coatings present a stable and effective long-term barrier in aggressive media and have a superior role over texture and wettability.

Author Contributions: Conceptualization, M.C. and P.G.; Methodology, M.C. and A.K.; Formal Analysis, M.C., A.K. and T.S.; Investigation, M.C. and T.S.; Writing—Original Draft Preparation, M.C. and A.K.; Writing—Review & Editing, M.C., A.K. and P.G.

Funding: This research was funded by the Slovenian Research Agency (research core funding Nos. P2-0132 and P2-0392 and project Nos. J2-7196 and J2-1741).

Acknowledgments: The authors acknowledge the support of SPI Lasers Ltd. by loan of their fiber laser within the research project Surface functionalization by nanosecond fiber laser texturing (nsFLaT).

Conflicts of Interest: The authors declare no conflict of interest.

References

1. Hryniewicz, T.; Rokicki, R.; Rokosz, K. Corrosion characteristics of medical-grade AISI Type 316L stainless steel surface after electropolishing in a magnetic field. *Corrosion* **2008**, *64*, 660–665. [CrossRef]
2. Ibrahim, M.A.M.; el Rehim, S.S.A.; Hamza, M.M. Corrosion behavior of some austenitic stainless steels in chloride environments. *Mater. Chem. Phys.* **2009**, *115*, 80–85. [CrossRef]
3. Long, J.Y.; Zhong, M.L.; Zhang, H.J.; Fan, P.X. Superhydrophilicity to superhydrophobicity transition of picosecond laser microstructured aluminum in ambient air. *J. Colloid Interface Sci.* **2015**, *441*, 1–9. [CrossRef] [PubMed]

4. Drzmala, J. Hydrophobicity and collectorless flotation of inorganic materials. *Adv. Colloid Interface Sci.* **1994**, *50*, 143–185. [CrossRef]
5. Long, J.Y.; Zhong, M.L.; Fan, P.X.; Gong, D.W.; Zhang, H.J. Wettability conversion of ultrafast laser structured copper surface. *J. Laser Appl.* **2015**, *27*, S29107. [CrossRef]
6. Kamegawa, T.; Irikawa, K.; Yamashita, H. Multifunctional surface designed by nanocomposite coating of polytetrafluoroethylene and TiO_2 photocatalyst: Self-cleaning and superhydrophobicity. *Sci. Rep.* **2017**, *7*, 13628. [CrossRef] [PubMed]
7. Xu, L.; Karunakaran, R.G.; Guo, J.; Yang, S. Transparent, superhydrophobic surfaces from one-step spin coating of hydrophobic nanoparticles. *ACS Appl. Mater. Interfaces* **2012**, *4*, 1118–1125. [CrossRef]
8. Zhang, L.; Zhao, N.; Xu, J. Fabrication and application of superhydrophilic surfaces: A review. *J. Adhes. Sci. Technol.* **2014**, *28*, 769–790. [CrossRef]
9. Zhang, X.; Jin, M.; Liu, Z.; Nishimoto, S.; Saito, H.; Murakami, T.; Fujishima, A. Preparation and photocatalytic wettability conversion of TiO_2-based superhydrophobic surfaces. *Langmuir* **2006**, *22*, 9477–9479. [CrossRef]
10. Lee, S.; Kim, W.; Yong, K. Overcoming the water vulnerability of electronic devices: A highly water-resistant ZnO nanodevice with multifunctionality. *Adv. Mater.* **2011**, *23*, 4398. [CrossRef]
11. Qing, Y.; Yang, C.; Sun, Y.; Zheng, Y.; Wang, X.; Shang, Y.; Wang, L.; Liu, C. Facile fabrication of superhydrophobic surfaces with corrosion resistance by nanocomposite coating of TiO_2 and polydimethylsiloxane. *Colloids Surf. A Physicochem. Eng. Asp.* **2015**, *484*, 471–477. [CrossRef]
12. Montemor, M.F. Functional and smart coatings for corrosion protection: A review of recent advances. *Surf. Coat. Technol.* **2014**, *258*, 17–37. [CrossRef]
13. Boinovich, L.B.; Emelyanenko, A.M.; Modestov, A.D.; Domantovsky, A.G.; Emelyanenko, K.A. Synergistic effect of superhydrophobicity and oxidized layers on corrosion resistance of aluminum alloy surface textured by nanosecond laser treatment. *ACS Appl. Mater. Interfaces* **2015**, *7*, 19500–19508. [CrossRef] [PubMed]
14. Ta, V.D.; Dunn, A.; Wasley, T.J.; Li, J.; Kay, R.W.; Stringer, J.; Smith, P.J.; Esenturk, E.; Connaughton, C.; Shephard, J.D. Laser textured superhydrophobic surfaces and their applications for homogeneous spot deposition. *Appl. Surf. Sci.* **2016**, *365*, 153–159. [CrossRef]
15. Gregorcic, P.; Setina-Batic, B.; Hocevar, M. Controlling the stainless steel surface wettability by nanosecond direct laser texturing at high fluences. *Appl. Phys. A Mater. Sci. Process.* **2017**, *123*, 766. [CrossRef]
16. Ta, V.D.; Dunn, A.; Wasley, T.J.; Li, J.; Kay, R.W.; Stringer, J.; Smith, P.J.; Esenturk, E.; Connaughton, C.; Shephard, J.D. Laser textured surface gradients. *Appl. Surf. Sci.* **2016**, *371*, 583–589. [CrossRef]
17. Ta, D.V.; Dunn, A.; Wasley, T.J.; Kay, R.W.; Stringer, J.; Smith, P.J.; Connaughton, C.; Shephard, J.D. Nanosecond laser textured superhydrophobic metallic surfaces and their chemical sensing applications. *Appl. Surf. Sci.* **2015**, *357*, 248–254. [CrossRef]
18. Kietzig, A.M.; Hatzikiriakos, S.G.; Englezos, P. Patterned Superhydrophobic Metallic Surfaces. *Langmuir* **2009**, *25*, 4821–4827. [CrossRef]
19. Gregorčič, P.; Conradi, M.; Hribar, L.; Hočevar, M.; Gregorcic, P.; Conradi, M.; Hribar, L.; Hocevar, M. Long-term influence of laser-processing parameters on (super)hydrophobicity development and stability of stainless-steel surfaces. *Materials* **2018**, *11*, 2240. [CrossRef]
20. Boinovich, L.B.; Gnedenkov, S.V.; Alpysbaeva, D.A.; Egorkin, V.S.; Emelyanenko, A.M.; Sinebryukhov, S.L.; Zaretskaya, A.K. Corrosion resistance of composite coatings on low-carbon steel containing hydrophobic and superhydrophobic layers in combination with oxide sublayers. *Corros. Sci.* **2012**, *55*, 238–245. [CrossRef]
21. Trdan, U.; Hocevar, M.; Gregorcic, P. Transition from superhydrophilic to superhydrophobic state of laser textured stainless steel surface and its effect on corrosion resistance. *Corros. Sci.* **2017**, *123*, 21–26. [CrossRef]
22. Emelyanenko, A.M.; Shagieva, F.M.; Domantovsky, A.G.; Boinovich, L.B. Nanosecond laser micro- and nanotexturing for the design of a superhydrophobic coating robust against long-term contact with water, cavitation, and abrasion. *Appl. Surf. Sci.* **2015**, *332*, 513–517. [CrossRef]
23. Fairley, N. *Casa XPS VAMAS Processing Software*; Casa Software Ltd.: Teignmouth, UK, 2018.
24. Conradi, M.; Drnovšek, A.; Gregorčič, P. Wettability and friction control of a stainless steel surface by combining nanosecond laser texturing and adsorption of superhydrophobic nanosilica particles. *Sci. Rep.* **2018**, *8*, 7457. [CrossRef] [PubMed]
25. McHale, G.; Shirtcliffe, N.J.; Newton, M.I. Super-hydrophobic and super-wetting surfaces: Analytical potential? *Analyst* **2004**, *129*, 284–287. [CrossRef]

26. Wang, Z.K.; Zheng, H.Y.; Lim, C.P.; Lam, Y.C. Polymer hydrophilicity and hydrophobicity induced by femtosecond laser direct irradiation. *Appl. Phys. Lett.* **2009**, *95*, 111110. [CrossRef]
27. Lai, J.N.; Sunderland, B.; Xue, J.M.; Yan, S.; Zhao, W.J.; Folkard, M.; Michael, B.D.; Wang, Y.G. Study on hydrophilicity of polymer surfaces improved by plasma treatment. *Appl. Surf. Sci.* **2006**, *252*, 3375–3379. [CrossRef]
28. Yang, Z.; Liu, X.; Tian, Y. Insights into the wettability transition of nanosecond laser ablated surface under ambient air exposure. *J. Colloid Interface Sci.* **2019**, *533*, 268–277. [CrossRef]